J Mater Sci (2011) 46:3550–3559
DOI 10.1007/s10853-011-5267-4

# Computational and electrochemical studies on the inhibition of corrosion of mild steel by L-Cysteine and its derivatives

**Jia-jun Fu · Su-ning Li · Ying Wang · Xiao-dong Liu · Lu-de Lu**

Received: 13 August 2010 / Accepted: 11 January 2011 / Published online: 29 January 2011


**Abstract** This article presents the investigation of L-Cysteine (CYS) and its derivatives including *N*-Acetyl-L-Cysteine (NACYS), *N*-Acetyl-*S*-Benzyl-L-Cysteine (NASBCYS), and *N*-Acetyl-*S*-Hexyl-L-Cysteine (NASHCYS) as green chemical corrosion inhibitors for mild steel in 1 M HCl solutions. Weight loss method and Tafel polarization measurement were performed to determine the corrosion parameters and inhibition efficiencies. Experimental results showed that these compounds suppressed both anodic and cathodic reactions, and the inhibition efficiency of the four inhibitors followed the order NASBCYS > NASHCYS > NACYS > CYS. In order to further study the corrosion mechanisms, quantum chemical calculation and molecular dynamics method were applied. The relationships between quantum chemical parameters and corrosion inhibition efficiency were discussed. Molecular dynamics method was used to simulate the adsorption behavior of each inhibitor in solvent. The results showed that these four inhibitors can adsorb on mild steel surface by donor acceptor interactions between lone-pair electrons of heteroatoms/$\pi$-electrons of aromatic ring and vacant *d*-orbital of iron.

## Introduction

Acidic aggressive solutions have been widely used for many industrial processes such as acid cleaning, pickling, and descaling [1–3]. The use of inhibitors is one of the most effective methods for metal protection against corrosion, especially in acidic environments [4, 5]. Most of the efficient acid inhibitors are organic compounds containing heteroatoms such as sulfur, nitrogen, phosphorus, and/or oxygen in their structures [6, 7]. These compounds can easily adsorb on metal surface, form a compact barrier film, and thus reduce the corrosion rate by chemisorption and physisorption processes. However, unfortunately most of the organic inhibitors have the toxic and carcinogenic properties [8, 9]. In response to more and more restrict environmental regulations, many researches are geared toward designing and synthesizing environmentally compatible and harmless corrosion inhibitors [10–13].

In the last few decades, the choice of the proper corrosion inhibitor was determined using the experimental means, which is very tedious, time-consuming, and expensive [14]. Recently, theoretical chemistry including quantum chemical calculation and molecular dynamic method has been employed to elucidate the inhibition mechanism and provide the theoretical basis for choosing the corrosion inhibitor [15–18]. Quantum chemical calculations are usually used to study the relationship between structure of the inhibitor molecule and its inhibition performance. However, it is usually suitable for calculating small systems containing no more than 100 atoms or small molecules [19]. On the contrary, molecular dynamic method, which is applied to explore the interaction of inhibitor molecules with the metal surface, is often used as a beneficial supplement of quantum chemical calculation. This method can provide a useful way to explain some important factors affecting corrosion process, such as nature of metal surface, solvent molecule, electrolyte anions, temperature, etc [20, 21]. So, we have sufficient reasons to believe that with the improvement of computer hardware and software technology, these two theoretical methods will play more important role in studying corrosion mechanisms.

J. Fu (✉) · S. Li · Y. Wang · X. Liu · L. Lu
School of Chemical Engineering, Nanjing University of Science and Technology, Nanjing 210094, Jiangsu, China
e-mail: fujiajun668@gmail.com

Cysteine, which is one of the naturally occurring amino acids, has been previously reported as an effective and green corrosion inhibitor for steel, copper, vanadium, and aluminum in various aggressive media [22–25]. Compared with the other amino acids, Cysteine shows better inhibition performance due to the existing of the mercapto groups in its structure, which can provide a strong affinity to adsorb on metal surface and block more active site during corrosion process. In this study, L-Cysteine and its derivatives (see in Table 1) have been studied as green corrosion inhibitors for mild steel in 1 M HCl solutions. The inhibition efficiency of these four amino acid compounds was investigated by chemical and electrochemical measurements. Another objective of this study is to correlate quantum parameters, such as the highest occupied molecular orbital ($E_{HOMO}$), the lowest unoccupied molecular orbital ($E_{LUMO}$), energy gap ($\Delta E$), dipole moment ($\mu$), molecular volume (MV), and the fraction of electrons transfer from inhibitors to iron ($\Delta N$) with experimental inhibition efficiencies of the four tested inhibitors. In addition, the adsorption behaviors of the four inhibitors on iron surface were studied using molecular dynamics simulation, and the adsorption energies were also calculated.

## Experimental

### Materials

L-Cysteine (CYS) and *N*-Acetyl-L-Cysteine (NACYS) were purchased from Acros Company. *N*-Acetyl-*S*-Benzyl-L-Cysteine (NASBCYS) and *N*-Acetyl-*S*-Hexyl-L-Cysteine (NASHCYS) were synthesized in the laboratory according to the previous literatures and characterized by $^1$H NMR

**Table 1** The chemical structures, names, abbreviations, and molecular weight of L-Cysteine and its derivatives

| Chemical structure | Name | Abbreviation | Molecular weight |
|---|---|---|---|
| 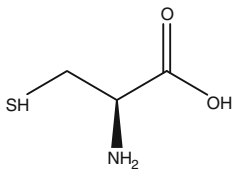 | L-Cysteine | CYS | 121.16 |
| 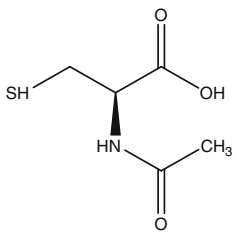 | *N*-acetyl-L-cysteine | NACYS | 163.19 |
| 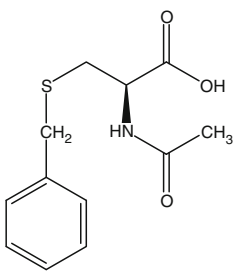 | *N*-acetyl-*S*-benzyl-L-cysteine | NASBCYS | 239.29 |
| 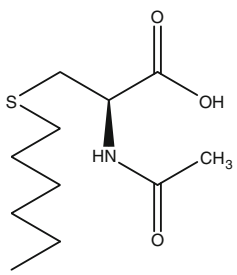 | *N*-acetyl-*S*-hexyl-L-cysteine | NASHCYS | 247.35 |

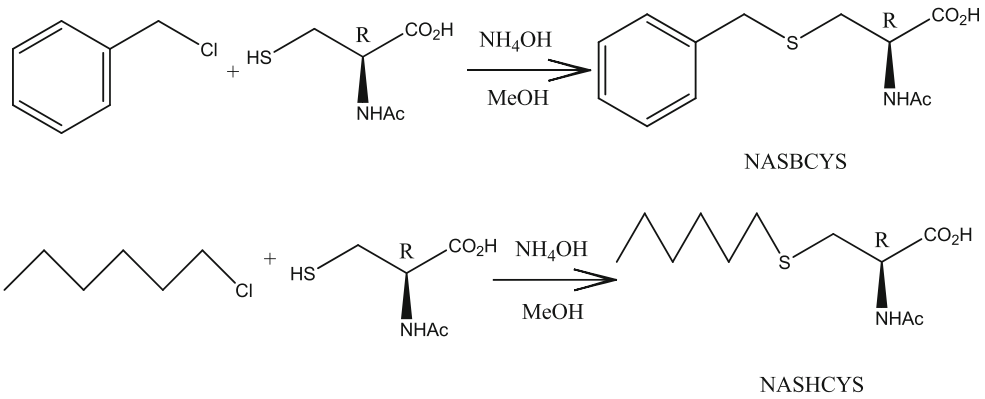


**Fig. 1** The synthetic route of NASBCYS and NASHCYS

spectroscopy [26, 27]. $^1$H NMR measurements were carried out in CDCl3 solutions using DRX300 (Bruker). The whole synthetic route is presented in Fig. 1.

$^1$H NMR for NASBCYS: $\delta$ (ppm) 2.0 (3H, s, CO–C*H*$_3$), 2.93 (2H, d, S–C*H*$_2$–CH *J* 4.2), 3.73 (2H, s, S–C*H*$_2$–Ar), 4.71 (1H, q, S–CH$_2$–C*H*, $J_1$ 5.2, $J_2$ 11.9), 6.19 (1H, d, CH–N*H*, *J* 7.0), 7.26–7.36 (5H, m, Ar–H).

$^1$H NMR for NASHCYS: $\delta$ (ppm) 0.89 (3H, t, *J* 6.6 Hz), 1.29–1.59 (8H, m), 2.11 (s, 3H, COC*H*$_3$), 2.55 (2H, t, S–C*H*$_2$–CH$_2$, *J* 7.3), 3.04 (2H, d, S–C*H*$_2$–CH, *J* 5.4), 4.80 (1H, m, S–CH$_2$–C*H*), 6.64 (1H, d, CH–N*H*–, *J* 7.0).

Corrosion tests were performed on a mild steel specimen of the following percentage composition (wt, %): 0.19C, 0.26Si, 0.58Mn, 0.05P, 0.06S, 0.08Cr, 0.03Mo, and the remainder iron. 1 M HCl solutions were prepared from an analytical reagent grade of 37% HCl and bidistilled water and used as aggressive media. The working electrode (WE) for electrochemical measurements was in the form of a rod machined into a cylindrical form embedded in epoxy resin leaving a working area of 0.5 cm$^2$ in contact with the test solution. The exposed surface of specimen was abraded using different grade emery papers (600, 800, 1500, and 2000), washed by double distilled water, degreased with acetone, and dried at room temperature before electrochemical use.

## Weight loss measurements

The pre-weighed mild steel specimens with uniform size (2 × 5 × 0.05 cm) were immersed in 500 ml 1 M HCl solutions in the absence and presence of inhibitors at different concentrations. All the test HCl solutions were isolated from air. After 2 h, the specimens were taken out, washed, dried, and weighed. Triplicate experiments were performed in each case, and the mean value of the weight loss was determined. The inhibition efficiency, IE$_W$ (%), was calculated using the following equation:

$$\mathrm{IE_W}(\%) = \frac{W_0 - W_1}{W_0} \times 100 \quad (1)$$

where $W_0$ and $W_1$ are the weight of the specimen in 1 M HCl solutions without and with the addition of inhibitor, respectively.

## Electrochemical measurements

The electrochemical measurements were carried out in a conventional three-electrode 500 mL cell assembly with specimens as WE, a platinum foil of 2.0 × 1.0 cm as counter electrode, and a saturated calomel electrode (SCE) provided with a Luggin capillary as reference electrode. The WE was placed vertically facing the counter electrode, and a reference electrode was placed near the WE. The temperature was maintained at 25 °C in all experiments by placing cell on a thermostated water bath. The WE was immersed in 1 M HCl solution for 30 min until a steady-state open circuit potential (OCP) was obtained. Electrochemical measurements were made using a PARSTAT 2273 potentiostat connected to a computer. The tested HCl solution was degassed with ultra-pure nitrogen bubbling for 30 min to avoid any reactions with dissolved oxygen. Tafel polarization scans were recorded by changing the electrode potential automatically from −250 to +250 mV versus OCP with a scan rate of 0.166 mV s$^{-1}$. The experiment data recordings and the calculation of the electrochemical parameters were performed using PowerSuite 2.58 Princeton software.

## Quantum chemical calculations

All the calculations were performed with the Gaussian 03W program [28]. The molecular structures of the four inhibitors were fully and geometrically optimized by density functional methods using the hybrid B3LYP functional with the 6-31G (*d*, *p*) orbital basis set. This basis set is well known to provide accurate geometries and electronic properties for a wide range of organic compounds [29]. It is well known that the phenomenon of electrochemical corrosion appears in the liquid phase. Therefore, in order to

ensure the accuracy of data, the solvent effect has to be taken into account in calculation. In this study, SCRF methods (self-consistent reaction field) were performed, using the polarized continuum method (PCM) as a model for solvent. In this model, solvent is treated as an expanse of dielectric media and the solute as a trapped molecule in a cavity surrounded by the solvent [30].

The following quantum chemical indices were calculated: $E_{HOMO}$, $E_{LUMO}$, $\Delta E$, $\mu$, TE, and MV.

The local reactivity of the molecule was analyzed through an evaluation of the Fukui indices, which are obtained from the electron density and useful to characterize donor–acceptor interactions [31]. The Fukui function $f(\vec{r})$ is defined as the derivative of the electronic density $\rho(\vec{r})$ with respect to the number of electrons $N$ at a constant external potential $v(\vec{r})$:

$$f(\vec{r}) = \left(\frac{\partial\rho(\vec{r})}{\partial N}\right)_{v(\vec{r})} \quad (2)$$

If the effects of relaxation associated with the addition or removal of electronic charges are not considered, then

$$\rho^{+}(\vec{r}) \approx \rho_{LUMO}(\vec{r}) \quad (3)$$

$$\rho^{-}(\vec{r}) \approx \rho_{HOMO}(\vec{r}) \quad (4)$$

where $\rho_{LUMO}(\vec{r})$ is the density of the lowest unoccupied molecular orbital and $\rho_{HOMO}(\vec{r})$ is density of the highest occupied molecular orbital.

The condensed Fukui functions are calculated by taking the finite difference approximations from Mulliken population analysis of atoms in inhibitor molecule, depending on the direction of the electron transfer:

$$f_k^{+} = q_k(N+1) - q_k(N) \quad \text{(for nucleophilic attack)} \quad (5)$$

$$f_k^{-} = q_k(N) - q_k(N-1) \quad \text{(for electrophilic attack)} \quad (6)$$

where $q_k$ is the gross charge of atom k in the molecule, and $N$ is the number of electrons. The condensed Fukui function is local reactivity descriptor and can be used only for comparing reactive atomic centers within the same molecule [32].

The condensed Fukui function calculations were performed with Materials Studio DMol$^3$ version 4.3, using a PBE (Perdew, Burke, and Enzerhof) functional and a double-numeric quality basis set with polarization functions (DND). Dmol$^3$ use a Mulliken population analysis.

### Molecular dynamics simulations

The molecular dynamics simulations were performed using the Discover molecular dynamics module in Material Studio 4.3 software from Accelrys Inc [33]. The surface Fe (1 1 0) was chosen to simulate the adsorption process. Interactions between the four investigated inhibitors and the Fe (1 1 0) surface were carried out in a simulation box (31.5 × 31.5 × 69.5 Å) with periodic boundary conditions to simulate a representative part of an interface devoid of any arbitrary boundary effects. The energy optimized inhibitor molecule, Fe (1 1 0) surface and water layers were constructed using the amorphous cell module. The molecular dynamics simulation was performed under 25 °C, NVT ensemble, with a time step of 1 fs and simulation time of 30 ps. Details of the simulation process have been reported elsewhere [34, 35].

The interaction energy $E_{Fe-inhibitor}$ between each inhibition molecule and the Fe surface was calculated according to the following equation:

$$E_{Fe-inhibitor} = E_{Total} - (E_{Fe} + E_{Inhibitor}) \quad (7)$$

where $E_{Total}$ is the total energy of the surface and inhibitor molecule. $E_{Fe}$ is the energy of Fe (1 1 0) surface without the inhibitor, and $E_{Inhibitor}$ is the energy of the inhibitor without the surface. Furthermore, the binding energy is the negative value of the interaction energy, $E_{binding} = -E_{Fe-inhibitor}$.

## Results and discussion

### Weight loss measurements

The effect of addition of CYS and its derivatives at different concentrations on the corrosion of mild steel in 1 M HCl solution was studied by weight loss measurements at 25 °C after 2 h of immersion period. Figure 2 shows the values of inhibition efficiencies obtained from weight loss measurement. The results show that all these compounds can reduce the corrosion rate of mild steel to some degree. When the concentration of each inhibitor increases, the

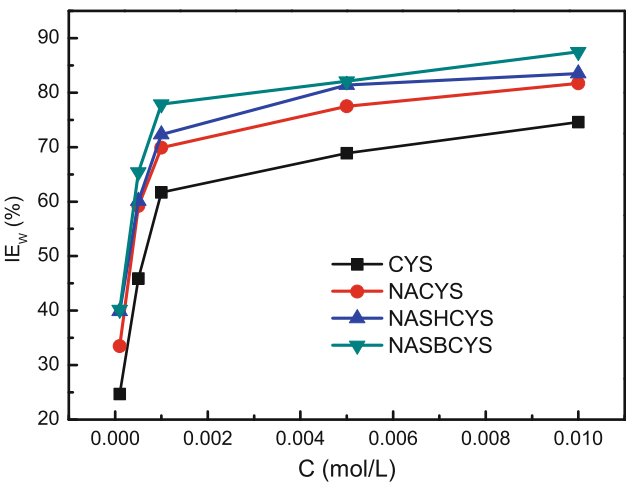


**Fig. 2** Inhibition efficiency of mild steel at various concentrations of L-Cysteine and its derivatives using weight loss measurements

inhibition efficiency also increases. This behavior is due to the fact that the adsorption capacity of inhibitor on the steel surface increases with the inhibitor concentration within the concentration range of $1 \times 10^{-4}$ to $1 \times 10^{-2}$ M. As for the four tested inhibitors, the inhibition efficiency increases in the order CYS < NACYS < NASHCYS <NASBCYS at the same concentration. The most effective corrosion inhibitor is NASBCYS, the highest inhibiton efficiency of 87.5% is achieved at $1 \times 10^{-2}$ M.

## Electrochemical measurements

Anodic and cathodic polarization curves for mild steel in 1 M HCl in the absence and presence of CYS, NACYS, NASBCYS, and NASHCYS at 25 °C are shown in Fig. 3a–d. Electrochemical corrosion kinetic parameters, such as corrosion potential ($E_{corr}$), corrosion current density ($j_{corr}$), and cathodic and anodic Tafel slope ($\beta_c$ and $\beta_a$) obtained by extrapolation of Tafel lines to the corrosion potential, are given in Table 2. The percentage inhibition efficiency, $IE_E$ (%), was calculated from the following equation and is also given in Table 2.

$$IE_E = \left(\frac{j^0_{corr} - j_{corr}}{j^0_{corr}}\right) \times 100 \quad (8)$$

where $j^0_{corr}$ and $j_{corr}$ are the corrosion current densities of mild steel in the presence and absence of inhibitor, respectively.

By comparing polarization curves in the absence and presence of various concentrations of the inhibitors, it can be easily seen that, in all cases, both the anodic and cathodic polarization curves shifted toward lower current density region after the addition of four inhibitors. These results show that the addition of these compounds to HCl solutions reduces the anodic dissolution of mild steel and also retards the cathodic hydrogen evolution reaction. It is also observed that the addition of inhibitors shifted slightly the $E_{corr}$ in the negative direction with reference to the blank solution. According to conclusion drawn by previous literatures [36, 37], if the displacement in corrosion potential is more than 85 mV with respect to corrosion potential of the blank, the inhibitor can be regarded as a cathodic or anodic type. The maximum displacement of the four tested inhibitors is 24.8 mV, indicating that CYS and its derivatives act as a mixed-type inhibitor but dominantly act as a cathodic inhibitor for mild steel in 1 M HCl.

From the Table 2, it is clear that the addition of each inhibitor decreases the corrosion rate of mild steel in 1 M HCl. The approximately constant values of $\beta$c and $\beta$a for the four inhibitors indicate that these compounds do not change the mechanism of iron dissolution and hydrogen evolution reaction. Like most organic corrosion inhibitors, these inhibitors adsorbed on steel surface by simply blocking the active sites. By comparing $j_{corr}$ values listed in Table 2, the conclusion can be drawn that CYS and its derivatives all show the good inhibition properties for the

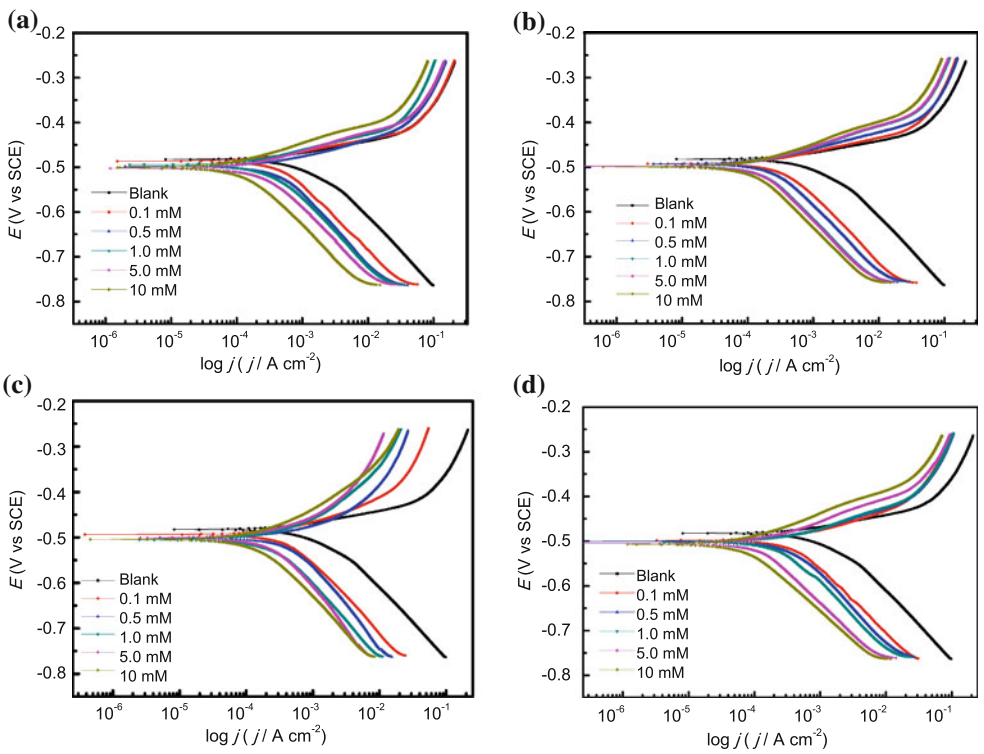


**Fig. 3** Anodic and cathodic polarization curves obtained for mild steel at 25 °C in 1 M HCl in various concentrations of tested inhibitors: **a** CYS, **b** NACYS, **c** NASBCYS, and **d** NASHCYS

**Table 2** Electrochemical polarization parameters for mild steel in the absence and presence of various concentrations of tested inhibitors in 1 M HCl

| Inhibitors | Concentration (M) | $j_{corr}$ (μA cm$^{-2}$) | $E_{corr}$ (mV) | $\beta_c$ (mV dec$^{-1}$) | $\beta_a$ (mV dec$^{-1}$) | $IE_E$ (%) |
|---|---|---|---|---|---|---|
| | Blank | 1150 | −482.1 | 125.3 | 59.7 | – |
| CYS | $1 \times 10^{-4}$ | 493 | −488.5 | 127.5 | 60.3 | 57.1 |
| | $5 \times 10^{-4}$ | 301 | −498.3 | 125.8 | 67.4 | 73.9 |
| | $1 \times 10^{-3}$ | 262 | −494.7 | 126.1 | 65.9 | 77.2 |
| | $5 \times 10^{-3}$ | 167 | −502.7 | 128.0 | 69.3 | 85.5 |
| | $1 \times 10^{-2}$ | 111 | −498.6 | 125.9 | 67.9 | 90.4 |
| NACYS | $1 \times 10^{-4}$ | 369 | −492.1 | 131.2 | 57.3 | 67.9 |
| | $5 \times 10^{-4}$ | 239 | −492.9 | 125.3 | 65.9 | 79.2 |
| | $1 \times 10^{-3}$ | 164 | −498.1 | 127.9 | 67.7 | 85.7 |
| | $5 \times 10^{-3}$ | 146 | −498.0 | 126.7 | 64.2 | 87.3 |
| | $1 \times 10^{-2}$ | 86 | −499.9 | 130.5 | 64.9 | 92.5 |
| NASBCYS | $1 \times 10^{-4}$ | 231 | −493.3 | 128.8 | 60.2 | 79.9 |
| | $5 \times 10^{-4}$ | 169 | −500.3 | 123.3 | 67.8 | 85.3 |
| | $1 \times 10^{-3}$ | 107 | −501.0 | 134.1 | 64.2 | 90.7 |
| | $5 \times 10^{-3}$ | 91 | −505.1 | 130.2 | 70.5 | 92.1 |
| | $1 \times 10^{-2}$ | 49 | −504.4 | 128.1 | 62.3 | 95.7 |
| NASHCYS | $1 \times 10^{-4}$ | 285 | −498.0 | 125.5 | 63.4 | 75.2 |
| | $5 \times 10^{-4}$ | 201 | −500.5 | 123.1 | 64.1 | 82.5 |
| | $1 \times 10^{-3}$ | 166 | −502.0 | 127.1 | 62.9 | 85.5 |
| | $5 \times 10^{-3}$ | 116 | −503.8 | 131.2 | 65.4 | 89.9 |
| | $1 \times 10^{-2}$ | 87 | −506.9 | 125.7 | 64.9 | 92.4 |

corrosion of mild steel in 1 M HCl and the efficiency of these inhibitors follow the order: NASBCYS > NASHCYS > NACYS > CYS. The inhibition efficiencies are in good agreement with that obtained from the weight loss measurements.

## Quantum chemical calculations

Quantum chemical methods, which can provide molecular level understanding of the corrosion mechanisms, have already been used to investigate the relationship between the structural properties of molecules and their inhibition performances. Geometric structures and electronic properties of four studied inhibitors were calculated by DFT method with 6-31G (*d*, *p*) basis set. The optimized molecular structures of the four studied molecules are shown in Fig. 4. Some quantum chemical parameters such as $E_{HOMO}$, $E_{LUMO}$, $\Delta E$, $\mu$, TE, and MV were presented in Table 3.

$E_{HOMO}$ and $E_{LUMO}$, which determine the order of difficulty the molecule interacts with other species, are very popular quantum chemical parameters [38]. According to the frontier molecular orbital theory, $E_{HOMO}$ often is associated with the electron donating ability of the molecule. High value of $E_{HOMO}$ is likely to indicate a tendency of the molecule to donate electrons to appropriate acceptor molecules of low empty molecular orbital energy. Similarly, $E_{LUMO}$ represents the ability of the molecule to accept electrons. The lower values of $E_{LUMO}$, the more probable the molecule accepts electrons [39]. In this study, the values of $E_{HOMO}$ show the order NASBCYS > NASHCYS > NACYS > CYS, while the values of $E_{LUMO}$ show the different orders NACYS = NASBCYS < NASHCYS < CYS. By comparing the inhibition efficiencies of the four inhibitors, it is not difficult to see that there was no direct relationship between inhibition efficiency and $E_{LUMO}$. However, there exists a good correlation between $E_{HOMO}$ and $\Delta E$ with inhibition efficiencies. The inhibition efficiency increases with decreasing $\Delta E$ and increasing of $E_{HOMO}$. An increase in the values of $E_{HOMO}$ can facilitate the adsorption, and therefore improved inhibition efficiency. NASBCYS has the lowest value of $\Delta E$, and thus the highest inhibition efficiency, which proves the fact that excellent corrosion inhibitors are usually those organic compounds who can not only offer electrons to unoccupied orbital of the metal, but also accept free electrons from the metal.

Dipole moment is the measure of polarity of a polar covalent bond. It is defined as the product of charge on the atoms and the distance between the two bonded atoms [40]. Dipole moment has been regarded as an important index to correlate with the inhibition efficiency. However, there still

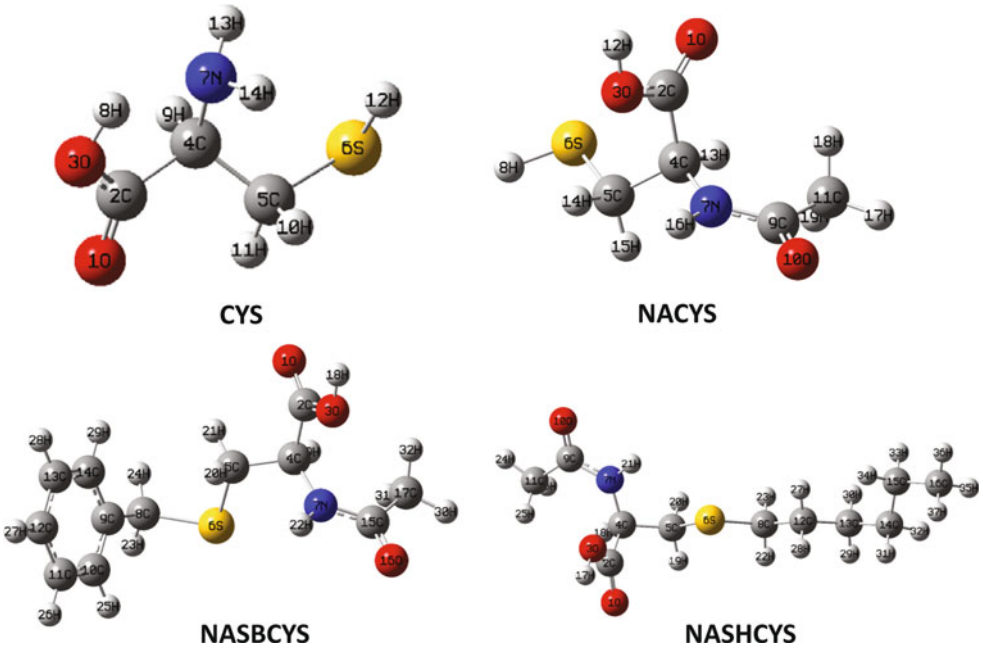


**Fig. 4** Optimized structures of CYS, NACYS, NASBCYS, and NASHCYS

**Table 3** Calculated quantum chemical parameters of CYS, NACYS, NASBCYS, and NASHCYS

| Molecule | Total energy (a.u.) | $E_{HOMO}$ (eV) | $E_{LUMO}$ (eV) | $\Delta E$ ($E_{LUMO} - E_{HOMO}$) (eV) | Dipole | Molar volume ($cm^3$ $mol^{-1}$) |
|---|---|---|---|---|---|---|
| CYS | −721.988 | −6.776 | −0.517 | 6.259 | 7.249 | 70.416 |
| NACYS | −874.660 | −6.680 | −0.735 | 5.945 | 5.043 | 112.781 |
| NASBCYS | −1145.046 | −6.422 | −0.735 | 5.687 | 5.573 | 199.530 |
| NASHCYS | −1110.562 | −6.449 | −0.706 | 5.743 | 5.102 | 193.179 |

exist the controversies with respect to the relationship between dipole moment and inhibition efficiency until now. Some author reported that an increase of the dipole moment has positive influence on the inhibition efficiency, while others obtained the opposite conclusion [41, 42]. In this study, the theoretical results indicated no direct relationship between $\mu$ and inhibition efficiency. CYS has the lowest inhibition efficiency among the inhibitors, which may be explained that too higher value of $\mu$ will prevent the accumulation of inhibitor molecules in mild steel surface. Furthermore, it is very obvious that the inhibition efficiency increases as the molecular volume increase, which is due to the increase of the contact area between molecule and surface. NASBCYS has the highest molecular volume with a value equals 199.530 $cm^3$ $mol^{-1}$, which probably makes a better surface coverage of the mild surface and thus prevents aggressive media from penetrating to surface. This is the other reason for the highest inhibition efficiency of NASBCYS.

According to Person [43], as a first approximation, the number of transferred electron, $\Delta N$, was also given by the equation as following:

$$\Delta N = \frac{\chi_{Fe} - \chi_{inh}}{2(\eta_{Fe} + \eta_{inh})} \quad (9)$$

where $\chi_{Fe}$ and $\chi_{inh}$ denote the absolute eletronegative of Fe and the inhibitor molecular, respectively; $\eta_{Fe}$ and $\eta_{inh}$ denote the absolute hardness of Fe and the inhibitor molecule, respectively. These quantities are related to electro affinity ($A$) and ionization potential ($I$) which are useful in their ability to help predict chemical behavior.

$$\chi = \frac{I + A}{2} \quad (10)$$

$$\eta = \frac{I - A}{2} \quad (11)$$

According to the theorem proposed by Koopman, the energies of the HOMO and LUMO orbitals of the inhibitor molecule are related in turn to $I$ and $A$ as following:

$$I = -E_{HOMO} \quad (12)$$

$$A = -E_{LUMO} \quad (13)$$

Values of $\chi$ and $\eta$ were calculated using the values of $I$ and $A$ obtained from quantum chemical calculations. Using

**Table 4** Quantum chemical descriptors for CYS, NACYS, NASBCYS, and NASHCYS

| Inhibitor | $I$ | $A$ | $\chi$ | $\eta$ | $\Delta N$ |
|---|---|---|---|---|---|
| CYS | 6.776 | 0.517 | 3.646 | 3.130 | 0.536 |
| NACYS | 6.680 | 0.735 | 3.708 | 2.973 | 0.554 |
| NASBCYS | 6.422 | 0.735 | 3.579 | 2.843 | 0.602 |
| NASHCYS | 6.449 | 0.706 | 3.778 | 2.872 | 0.561 |

a theoretical $\chi$ value of 7 eV $mol^{-1}$ and $\eta$ value of 0 eV $mol^{-1}$ for iron atom, $\Delta N$, which is the fraction of electrons transferred from inhibitor to the mild steel surface was calculated and the results were shown in Table 4. According to Lukovits [44], if $\Delta N < 3.6$, the inhibition efficiency increased with increasing electron donating ability at the metal surface. In this study, the CYS and its derivatives were the donators of electrons, and the iron surface was the acceptor. It can be inferred that these inhibitors can adsorb on mild steel surface on the basis of donor–acceptor interactions between the lone-pair electrons of the heteroatoms/$\pi$-electrons of the benzene ring and the vacant $d$-orbitals of the metal surface. From Table 4, the values of $\Delta N$ show the relation NASBCYS > NASHCYS > NACYS > CYS for this property. This result is completely agreement with the order of electron donating ability of these inhibitors reflected by $E_{HOMO}$.

The local reactivity is analyzed by means of the condensed Fukui functions, which allow us to distinguish each part of the molecule on the basis of its distinct chemical behavior due to the different substituent functional groups. Thus, the site for nucleophilic attack will be the place where the value of $f_k^+$ is a maximum. In turn, the site for electrophilic attack is controlled by the value of $f_k^-$. The values of the Fukui functions for a nucleophilic and electrophilic attack are given for the three inhibitors in Table 5. (only for nitrogen, sulfur, oxygen, and carbon atoms)

Careful examination of the Fukui indices presented in Table 5 shows that all the inhibitors have only one reactive site for electrophilic attack located on the sulfur atom, which can be proved by the distribution of HOMO showed in Fig. 5. As for sites prone to nucleophilic attacks, in all case the O1, C2, and O3 atoms of the carboxylic acid group has the highest values of $f_k^+$ ranged from 0.112 to 0.259. In addition, there exist the other probable sites susceptible to nucleophilic attack: C9, C10, and C12 in aromatic ring in NASBCYS molecule. Figure 5 also presents the distribution of LUMO for the four inhibitors. From Fig. 5, it can also be seen that the LUMO is located not only in the carboxylic acid groups but also in the benzene ring, which is consistent with the atoms that exhibit the greatest value of $f_k^+$.

## Molecular dynamics simulations

The molecular dynamics simulations were performed to investigate the adsorption behavior of the CYS and its derivatives on mild surface at the molecular level. The four

**Table 5** Calculated Fukui functions for CYS, NACYS, NASBCYS, and NASHCYS

| Number | CYS | | | NACYS | | | NASBCYS | | | NASHCYS | | |
|---|---|---|---|---|---|---|---|---|---|---|---|---|
| | Atom | $f_k^+$ | $f_k^-$ | Atom | $f_k^+$ | $f_k^-$ | Atom | $f_k^+$ | $f_k^-$ | Atom | $f_k^+$ | $f_k^-$ |
| 1 | O | 0.199 | 0.056 | O | 0.221 | 0.028 | O | 0.122 | 0.015 | O | 0.229 | 0.019 |
| 2 | C | 0.259 | 0.027 | C | 0.247 | −0.006 | C | 0.152 | 0.007 | C | 0.259 | −0.006 |
| 3 | O | 0.112 | 0.025 | O | 0.114 | 0.009 | O | 0.061 | 0.008 | O | 0.114 | 0.010 |
| 4 | C | −0.036 | −0.027 | C | −0.019 | −0.010 | C | −0.028 | 0.009 | C | −0.042 | −0.001 |
| 5 | C | −0.038 | −0.029 | C | −0.017 | −0.031 | C | −0.012 | 0.037 | C | −0.030 | −0.035 |
| 6 | S | 0.117 | 0.585 | S | 0.043 | 0.638 | S | 0.078 | 0.492 | S | 0.063 | 0.592 |
| 7 | N | 0.000 | 0.037 | N | −0.002 | −0.001 | N | −0.006 | 0.004 | N | −0.004 | −0.008 |
| 8 | | | | H | – | – | C | 0.004 | 0.039 | C | −0.002 | −0.031 |
| 9 | | | | C | 0.045 | 0.013 | C | 0.036 | 0.009 | C | 0.013 | 0.006 |
| 10 | | | | 0 | 0.060 | 0.038 | C | 0.043 | 0.021 | O | 0.029 | 0.015 |
| 11 | | | | C | −0.010 | −0.002 | C | 0.017 | 0.018 | C | −0.011 | −0.003 |
| 12 | | | | | | | C | 0.072 | 0.027 | C | −0.007 | −0.014 |
| 13 | | | | | | | C | 0.030 | 0.022 | C | −0.002 | −0.008 |
| 14 | | | | | | | C | 0.023 | 0.016 | C | −0.001 | −0.004 |
| 15 | | | | | | | C | 0.010 | 0.008 | C | −0.001 | −0.002 |
| 16 | | | | | | | O | 0.019 | 0.018 | C | 0.000 | 0.000 |
| 17 | | | | | | | C | −0.006 | 0.003 | | | |

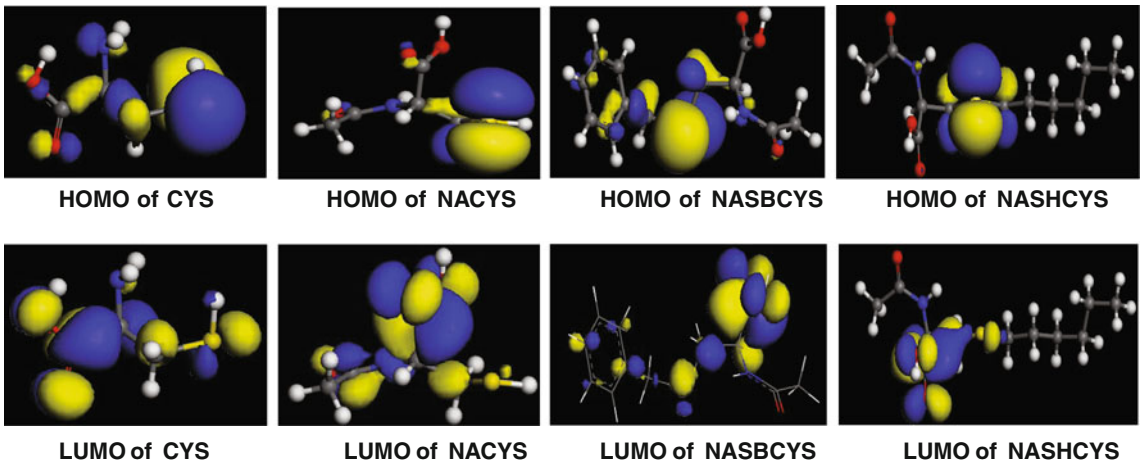


**Fig. 5** Frontier molecular orbital diagrams of CYS, NACYS, NASBCYS, and NASHCYS

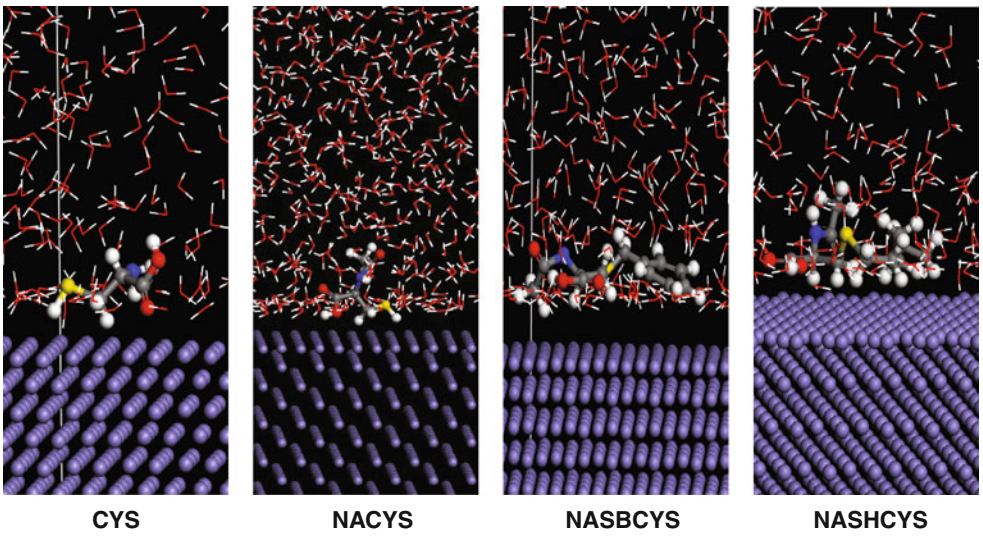


**Fig. 6** Equilibrium adsorption configurations of the four inhibitors on Fe (1 1 0) surface

inhibitors adsorbed on the mild steel surfaces after adsorption equilibrium are shown in Fig. 6. It can be seen from Fig. 6 that the final configurations of the four inhibitors thoroughly changed as compared with the corresponding initial configurations. The final configurations of CYS and NACYS show that O1, C2, O3, and S6 with the maximum values of $f_k^+$ or $f_k^-$ are very close to the steel surface, which indicate that these molecules adsorbed on the steel surface by electrons transfer between metal surface and reactive sites of the molecules. Figure 6 also shows that the NASBCYS molecule is in the planar manner and nearly parallel to the mild steel surface. By analysis of the final configuration, we can draw the conclusion that the NASBCYS adsorbed on the steel surface through not only the active heteroatoms but also the aromatic ring. Both interactions can make it form strong coordinated bonds with iron. In addition, for NASHCYS, besides relying on the good adhesive abilities of reactive sites (O1, C2, and O3 atoms), the non-polar long carbon chain was also parallel to the surface and covered the maximum area of metal surface.

The values of adsorption energy and binding energy obtained from the molecular simulation program were calculated and tabulated in Table 6. The binding energy for NASBCYS was the highest and equals to 397.76 kJ $mol^{-1}$. The higher the value of bind energy is, the stronger bonds between inhibitors and metal surface are formed, and the higher inhibition efficiency is. High value of binding energy indicates that the NASBCYS will give the higher inhibition efficiency, which is consistent with the inhibition efficiency obtained from the electrochemical technique.

**Table 6** Interaction and binding energy of the four inhibitors on Fe (1 1 0) surface

| Inhibitor | $E_{\text{Fe–inhibitor}}$ (kJ mol$^{-1}$) | $E_{\text{binding}}$ (kJ mol$^{-1}$) |
|---|---|---|
| CYS | −294.70 | 294.70 |
| NACYS | −311.45 | 311.45 |
| NASBCYS | −397.76 | 397.76 |
| NASHCYS | −389.12 | 389.12 |

## Summary and conclusion

The following conclusions are drawn from this study:

(1) CYS and its derivatives are efficient inhibitors for corrosion of mild steel in 1 M HCl solution.

(2) All the investigated inhibitors act as mixed-type inhibitor, and the inhibition efficiency order for inhibitor is NASBCYS > NASHCYS > NACYS > CYS under the same condition.

(3) Data obtained from quantum chemical calculations were related to the experimental inhibition efficiency. No significant relationship was found between $E_{\text{LUMO}}$ and $\mu$ with the experimental inhibition efficiency. However, $E_{\text{HOMO}}$, $\Delta E$, and MV are good quantities to correlate with experimental inhibition efficiency.

(4) The molecular dynamics simulation results show that the four inhibitors can adsorb on the Fe (1 1 0) surface through heteroatoms (nitrogen, oxygen, and sulfur atoms) and/or $\pi$-electrons in the aromatic ring.

**Acknowledgements** The authors are pleased to acknowledge the financial support provided by Specialized Research Fund for the Doctoral Program of Higher Education, China (No. 20093219120014) and NUST Research Funding, China (No. 2010ZYTS016).

## Reference:

1. Nwaogu UC, Blawert C, Scharnagl N, Dietzel W, Kainer KU (2010) Corros Sci 52:2143
2. Abdel-Karim R, El-Raghy SM, Waheed AAF, Abdel-Momen SST (2009) Mater Perform 48:46
3. Sathiyanarayanan S, Jeyaprabha C, Muralidharan S, Venkatachari G (2006) Appl Surf Sci 252:8107
4. Behpour M, Ghoreishi SM, Gandomi-Niasar A, Soltani N, Salavati-Niasari M (2009) J Mater Sci 44:2444. doi:10.1007/s10853-009-3309-y
5. Umoren SA, Obot IB, Obi-Egbedi NO (2009) J Mater Sci 44:274. doi:10.1007/s10853-008-3045-8
6. Prabhu RA, Venkatesha TV, Shanbhag AV (2009) J Iran Chem Soc 6:353
7. Ostovari A, Hoseinieh SM, Peikari M, Shadizadeh SR, Hashemi SJ (2009) Corros Sci 51:1935
8. Zhang DQ, Cai QR, He XM, Gao LX, Kim GS (2009) Corros Sci 51:2349
9. Yu H, Chen B, Wu H, Sun X, Li B (2008) Electrochim Acta 54:720
10. Obot IB, Obi-Egbedi NO (2010) J Appl Electrochem 40:1977
11. Oguzie EE (2008) Corros Sci 50:2993
12. Quraishi MA, Singh A, Singh VK, Yadav DK, Singh AK (2010) Mater Chem Phys 122:114
13. Ghareba S, Omanovic S (2010) Corros Sci 52:2104
14. Jamalizadeh E, Jafari AH, Hosseini SMA (2008) J Mol Struct THEOCHEM 870:23
15. Şahin M, Gece G, KarcI F, Bilgiç S (2008) J Appl Electrochem 38:809
16. Rayat S, Chhabra R, Alawode O, Gundugola AS (2009) J Mol Struct 933:38
17. Oguzie EE, Enenebeaku CK, Akalezi CO, Okoro SC, Ayuk AA, Ejike EN (2010) J Colloid Interface Sci 349:283
18. Fu JJ, Li SN, Cao LH, Wang Y, Yan LH, Lu LD (2010) J Mater Sci 45:979. doi:10.1007/s10853-009-4028-0
19. Gece G, Bilgiç S (2009) Corros Sci 51:1876
20. Tang Y, Yang X, Yang W, Chen Y, Wan R (2010) Corros Sci 52:242
21. Liu J, Yu W, Zhang J, Hu S, You L, Qiao G (2010) Appl Surf Sci 256:4729
22. Fu JJ, Li SN, Wang Y, Cao Lh, Ld Lu (2010) J Mater Sci 45:6255. doi:10.1007/s10853-010-4720-0
23. Saifi H, Bernard MC, Joiret S, Rahmouni K, Takenouti H, Talhi B (2010) Mater Chem Phys 120:661
24. El-Rabiee MM, Helal NH, Abd EI-Hafez GhM, EI-Hafez GMA, Badawy WA (2008) J Alloys Compd 459:466
25. Kiani MA, Mousavi MF, Ghasemi S, Shamsipur M, Kazemi SH (2008) Corros Sci 50:1035
26. Hickman RJS, Christie BJ, Guy RW, White TJ (1985) Aust J Chem 38:899
27. Sano K, Ikegami Y, Uesugi T (2001) Biol Pharm Bull 24:1324
28. Levine IN (1991) Quantum chemistry. Prentice Hall, New Lersey
29. John S, Joseph B, Balakrishnan KV, Aravindakshan KK, Joseph A (2010) Mater Chem Phys 123:218
30. Barone V, Cossi M (1998) J Phys Chem A 102:1995
31. Cruz J, Martínez-Aguilera LMR, Salcedo R, Castro M (2001) Int J Quantum Chem 85:546
32. Lesar A, Milošev I (2009) Chem Phys Lett 483:198
33. Xia S, Qiu M, Yu L, Liu F, Zhao H (2008) Corros Sci 50:2021
34. Amin MA, Khaled KF, Fadl-Allah SA (2010) Corros Sci 52:140
35. Khaled KF (2009) J Solid State Electrochem 13:1743
36. Ferreira ES, Giancomelli C, Giacomelli FC, Spinelli A (2004) Mater Chem Phys 83:129
37. Riggsjr OL (1973) Corrosion inhibitor, 2nd edn. Nathan, Houston
38. Fukui K (1975) Theory of orientation and stereoselection. Springer, New York
39. Fang J, Li J (2002) J Mol Struct THEOCHEM 593:179
40. Kikuchi O (1987) Quant Struct Act Relat 6:179
41. Lagrenée M, Mernari B, Chaibi N, Traisnel H, Vezin H, Ben (2001) Corros Sci 43:951
42. Stoyanova A, Petkova G, Peyerimhoff SD (2002) Chem Phys 279:1
43. Person PG (1986) Proc Natl Acad Sci 83:8440
44. Lukovits I, Kalman E, Zucchi F (2001) Corrosion 57:3